Original Article

Computed tomographic contrast enhancement and tumor angiogenesis in canine oral tumors

Urapa Klansnoh[1] Wijit Banlunara[2] Nan Choisunirachon[1*]

Abstract

The potential value of bolus tracking contrast enhanced computed tomography (CT) in the diagnosis of oral tumors in dogs was investigated by examining the relationship between contrast-enhanced CT image density and microvascularization. Among 20 dogs with oral tumors, aged 8 – 17 years, weight 3.6 – 40.0 kg, 13 dogs were suffering with melanoma (MM), 4 with squamous cell carcinoma (SCC), and 3 with fibrosarcoma. Based on contrast-enhanced CT scan, the time lag from the injection of contrast medium into the right cephalic vein until the contrast medium returned to the mid-cervical external jugular vein at the level of the 4th cervical vertebrae significantly correlated with body weight ($p < 0.01$). The mean of post-contrast-enhancement increase in intra-tumor image density, measured in Hounsfield Units (HU), was 127.09 ± 38.58%, with the highest values detected in SCC (166.88 ± 23.47%, $p < 0.05$), followed by MM (122.78 ± 37.90%) and fibrosarcoma (99.37 ± 31.58%). The mean of microvessel density (MVD, a measure of vascularization determined by vWF-immunohistochemistry) of all tumors was 36.7 ± 11.7 vessels/mm^2, with the highest MVD values in SCC (47.5 ± 5.3 vessels/mm^2, $p < 0.05$), followed by MM (35.3 ± 11.6 vessels/mm^2) and fibrosarcoma (27.2 ± 6.5 vessel/mm^2). The values for MVD and intra-tumor HU in post-contrasted-enhanced CT scans significantly correlated ($p < 0.01$).

Keywords: angiogenesis, computed tomography, dog, oral, tumor

[1]*Department of Veterinary Surgery, Faculty of Veterinary Science, Chulalongkorn University, Bangkok, Thailand, 10330*
[2]*Department of Pathology, Faculty of Veterinary Science, Chulalongkorn University, Bangkok, Thailand, 10330*
***Correspondence**: nan.c@chula.ac.th*

Introduction

In canine patients, oral tumors can be found in areas such as the oral mucosa, gingiva, palate, tongue and tonsils. Generally, the malignancy of an oral tumor is a function of the tumor cell origin. Oral tumors can be benign, such as epulis or papilloma, but most canine oral tumors are malignant. The majority of malignant tumors are malignant melanomas (MM) but squamous cell carcinoma (SCC) and fibrosarcoma are also reported frequently (Niemiec, 2008). Because these types of tumors are characterized by high growth rate and invasiveness, it is essential that precise diagnoses and clinical staging be determined prior to the initiation of treatment.

In clinical practice, oral tumor location and invasion may ordinarily be assessed using basic diagnostic images such as skull radiographs. However, due to the superimposed bony tissue, precise information is difficult to obtain in this way. Currently, advanced diagnostic imaging techniques such as computed tomography (CT) are increasingly being applied in veterinary medicine. CT has the advantage of providing multi-planar images from the volumetric data of the patient, which eliminates the conventional radiographic limitation, especially in the head and neck area. When analyzed on a computer, CT data can be displayed in several grey scales, enhancing the ability of a veterinarian to detect any anatomical lesions (Ohlerth and Scharf, 2007). In addition to conventional CT scanning, intravenous iodinated contrast medium can be used to reveal highly vascularized lesions (Miles et al., 2012), which is helpful in investigating the affected area in disorders such as inflammatory diseases and tumors.

It is well known that tumor neovascularization plays an important role in tumor growth and metastasis. Several researchers have demonstrated that tumor angiogenesis, detected via intra-tumoral microvessel density (MVD), can be used as one of the malignant indicators (Weidner, 1995; Restucci et al., 2003; Wolfesberger, et al., 2008). Although MVD has been shown to be a good indicator of tumor malignancy, it has had the disadvantage that assessment requires invasive procedures such as tissue biopsy or tumor resection for histopathology. Ouyang et al. (2017) have reported that the intensity of a contrast-enhanced CT image, measured by Hounsfield Unit (HU) attenuation number, can provide an estimator of MVD in renal cell carcinoma. Despite the disagreement of CT value observed through the attenuation number and density including the area of microvessels detecting on different renal cell carcinoma (RCC) subtypes which were clear cell RCC and papillary RCC, overall findings suggest that contrast-enhanced CT images could be clinically advantageous for malignancy assessment. In companion animals, several studies have reported the utilization of contrast-enhanced CT images for detecting the anatomical alteration from maladies of the head and neck (Codner et al., 1993; Drees et al., 2009; Ghirelli et al., 2013). Nevertheless, non-dynamic, contrast-enhanced CT images were less advantageous for malignancy estimation (Kafka et al., 2004). Camp et al. (2000) has reported that the dynamic contrast-enhanced CT estimation technique for canine nasal tumors could be applied as the oxygenation parameter prior radiation procedure. However, the previous technique has limitations due to the fact that the acquisition data was derived from only a small area of selected tumor tissue. Since canine oral tumors are frequently presented in aging companion pets other diagnostic procedure revealed less information for prognosis and treatment manner. Therefore, the aims of this study were (1) to develop a diagnostic imaging technique by means of bolus tracking contrast-enhanced CT images for canine head and neck tumors that can be applied as a prospective estimator of tumor malignancy through the tumor vascularization in related different size of dog breeds, (2) to investigate the correlation between HU attenuation number of an oral tumor after contrast-enhanced CT and tumor angiogenesis as quantified by MVD, and (3) to compare the attenuation numbers with the MVD for various types of oral tumors, tumor location and tumor staging.

Materials and Methods

Animals: 20 canine oral tumor patients presented at the oral surgical unit, The Small Animal Teaching Hospital, Faculty of Veterinary Science, Chulalongkorn University between March 2014 and November 2015 were enrolled in this study. All dogs were clinically examined and confirmed to be affected by oral neoplasia. If a patient had been treated by surgical resection or chemotherapy, the dog was excluded from the study. All available information concerning the enrolled dogs, including history, symptoms, physical examination results, oral tumor evaluation and laboratory data, was recorded. In addition, the affected dogs in this study were clinical staged in accordance with the tumor size and the regional metastatic status from lymph node biopsy at the time of oral mass removal and the distant metastatic status from whole body metastatic screening through CT images.

This study was approved by the Institutional Animal Care and Use Committee (IACUC) in accordance with university regulations and policies governing the care and use of laboratory animals, and consent was obtained from each dog owner. The animal use protocol number was 1431045.

Computed tomography: Prior to CT examination, all dogs were examined to confirm that hematologic and serum biochemistry results were within normal limits for anesthetic procedures. On the day of CT examination, all dogs fasted for 8 hours and intravenous fluid rehydration was given using a crystalloid solution (Acetar®, 10 ml/kg/hour) through the right cephalic vein. The dog was then sedated with diazepam (Diapine®, Atlantic laboratories, Thailand, 0.3 mg/kg) intravenously. Subsequently, general anesthesia was induced using propofol (Lipuro®1%, Melsungen, Germany, 6 - 10 mg/kg, IV). After endotracheal intubation, the dogs were maintained under general anesthesia using 2 – 5% isoflurane (Isofurane®, Bethlehem, U.S.A.). The dog was placed on the CT bed (64-slice helical CT unit; Optima

CT660®, GE, Thailand) with its head pointing into the gantry and all forelegs caudally positioned. The center of the skull was set at the isocenter. After the pre-scan phase, the field of view (FOV) was set to cover the whole area extending from the nostril to the 7th cervical vertebra, and the pre-contrast scan was acquired using the following parameters: slice thickness = 0.625 mm, pitch = 0.531 mm per tube rotation; 120 kVp; 100 mA. Before the post-contrast-enhanced CT images were obtained, a region of interest (ROI) was designated at either the right or left external jugular vein at the mid 4th cervical vertebra. The contrast medium, using iohexol (Omnipaque®, Cork, Ireland, 600 mgI/kg), was administered through the right cephalic vein by automatic injector (2 ml/sec). Once the HU number in the specified ROI reached 100 HU, post-contrast CT images were recorded (Fig. 1). All CT data, including the lag period from contrast medium injection until the enhanced HU reached 100 HU at the mid-cervical external jugular vein, were recorded in Digital Imaging and Communications in Medicine (DICOM) files, and analyzed using Osirix® software (Osirix®, Geneva, Switzerland) at the workstation. To determine the HU numbers comparing pre- and post- contrast enhancement, CT images were viewed on a soft tissue window (WW = 75 HU and WL = 450 HU). Small ROIs were randomly drawn on the oral tumor in 5 areas and the HU number at each area was recorded. In the case of mineralized tumor tissue, mineralized areas were omitted. To reproduce the same locations for comparisons of HU numbers between the pre- and post-contrast-enhanced CT series, the ROIs of the pre-contrast-enhanced series were saved and then imported into the post-contrast-enhanced CT. The percentage of post-contrast enhancement was calculated using the formula (Post-contrast-enhanced HU – Pre-contrast-enhanced HU x 100 / Pre-contrast-enhanced HU).

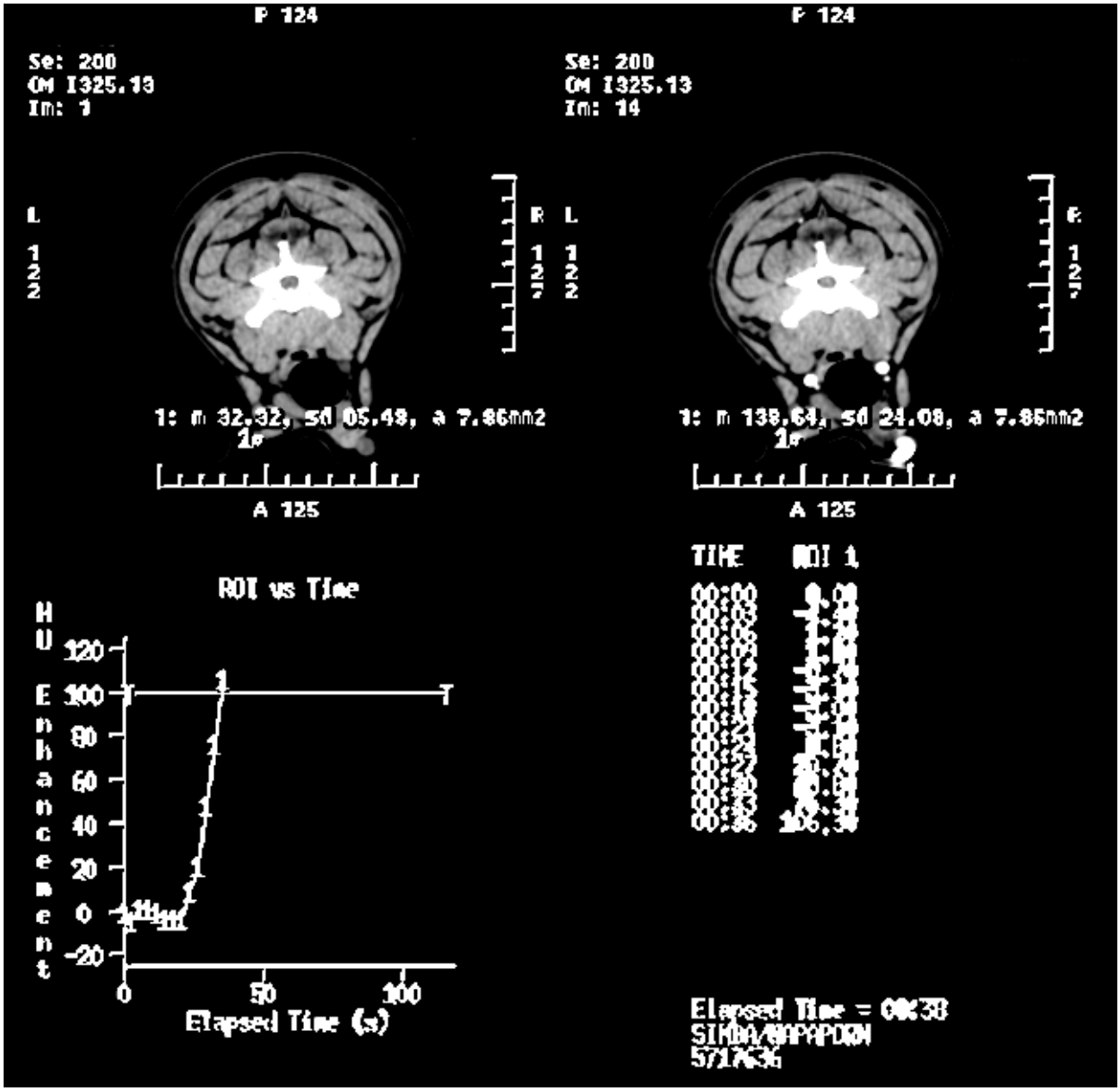

Figure 1 Dynamic contrast-enhanced computed tomographic (CT) image for canine head and neck area. The region of interest (ROI) on a mid-cervical CT image was drawn at the cervical jugular vein at the level of the 4th cervical vertebra. As soon as the contrast was circulated to the ROI such that the value reached 100 Hounsfield unit (HU), a post-contrast-enhanced CT scan was acquired. The time lag from injection of the contrast medium into the right cephalic vein until the 100 HU enhancement was detected at the ROI was noted and compared between dogs.

Histopathology and microvessel density: As soon as the CT procedure had finished, the dogs were subjected to oral mass resection. After surgical resection of the oral tumor, a 1 cm^3 sample was excised from the tumor mass and fixed in 10% neutral buffered formalin for 24 h prior to tissue processing for histopathologic investigation. A series of 4 µm thick sections were then stained with hematoxylin-eosin with special staining; Masson Fontana for melanin pigment and Mason Trichome for fibrous tissue; or immune-stained for endothelial cells using polyclonal rabbit anti-human Von Willebrand factor (vWF; Dako, Glostrup, Denmark). Briefly, after deparaffinization in xylene and rehydration in graded ethanol, section slides were washed with distilled water and phosphate buffer saline (PBS) solution. In cases of MM, samples were demelanized by incubating in 0.25 % potassium permanganate for 45 min followed by an oxalic acid solution for 3 min. Then, all samples were immune-stained using the chain polymer conjugated method. To retrieve protein antigens from samples, section slides were incubated in a sodium citrate buffer, pH 6.4, for 5 min using the heat-mediated, microwave method. Endogeneous peroxide was then inactivated by incubating the section slides with 3% hydrogen peroxidase. After washing with PBS, non-specific protein binding was saturated by normal blocking serum, using 8% skimmed milk in PBS at room temperature for 30 min. Subsequently the section slides were incubated with vWF (1:200) at 4° C overnight. The samples were then washed and labeled with a chained polymer solution containing HRP-conjugated antibodies against rabbit IgG (EnVisionTM-HRP labeled polymer, DAKO) for 45 min. Tissue sections were visualized using a liquid DAB/hydrogen peroxidase solution (DAKO). Nuclear counter-staining of each section was done by Mayer's hematoxylin before dehydration by graded ethanol, clearing in xylene and covering with a cover-glass. Renal tissue was applied as a positive control, while primary antibody replacement with PBS was used as a negative control.

To evaluate the MVD expression of each sample by veterinary pathologists, 5 "hot spots" which were the most condense vWF-immune-stained vessels on the tissue were primarily selected at 40x magnification, and the density of vWF-positive vessel (vessel/mm^2), defined as the MVD expression for each hot spot area, was then recorded at 100x magnification.

Statistical analysis: All data were analyzed using Prism7 (Graphpad software, California, USA). Measurements were expressed as mean and standard deviation. The correlation between canine body weight and the time lag from injection of the contrast medium until the contrast medium showed up at the mid-cervical jugular vein was analyzed using the Pearson correlation test. The MVD number and the percentage of post-contrast-enhanced HU among tumor groups were compared using a Kruskal-Wallis test. The correlation between the MVD number and the percentage of post-contrast-enhanced HU was analyzed using the Pearson correlation test. Tests with $p < 0.05$ were defined as statistically significant.

Results

Clinical demographic data: Among the 20 canine patients with oral tumors, there were 15 males (12 intact and 3 castrated) and 5 females (2 intact and 3 neutered). The average age was 12.0 ± 2.3 years old (8 – 17 years old). The average body weight was 15.5 ± 12.0 kg (3.6 – 40.0 kg). There were 6 Poodles, 4 mixed breed dogs, 2 Pugs, 2 Golden retrievers, 2 Thai dogs and 1 Shitzu, Rottweiler, German shepherd and terrier. Histologically, 13 dogs were affected by MM, 4 by SCC, and 3 by fibrosarcoma.

The most frequent location of oral tumors was the gingiva (13 dogs), followed by lip (5 dogs), buccal mucosa (1 dog), and hard palate (1 dog). After clinical staging in accordance with world health organization criteria by means of tumor size and tumor invasion either of regional or distant area, 5 dogs were found to be at clinical stage II (2 dogs with MM, 2 with SCC, and 1 with fibrosarcoma), 1 dog was at clinical stage III (MM), and 14 dogs were at clinical stage IV (10 dogs with MM, 2 with SCC, and 2 with fibrosarcoma).

Computed tomographic data: The time lag from injection of the contrast medium into the right cephalic vein until the HU reached 100 at the mid-cervical external jugular vein ranged from 15.0 to 49.0 seconds (mean 17.11 ± 12.26 seconds). The time lag strongly correlated with the body weight (range 3.8 to 40.0 kg) of the canine patients (R = 0.87, $p < 0.01$; Fig. 2).

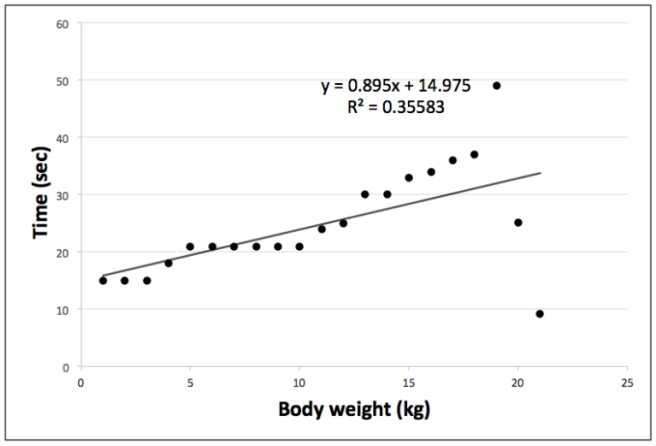

Figure 2 Correlation between body weight of canine patients and time lag between injection of contrast medium into the right cephalic vein and circulation of the contrast medium to the mid-cervical jugular vein.

The mean percentage increase in post-contrast-enhanced HU attenuation number at the soft tissue of the oral tumor areas compared to the pre-contrast-enhanced CT images was 127.09 ± 38.58% (range 62.90 – 196.00%). From the results, locations and clinical stages of tumors were not effected to the CT attenuation number. By location, between gingival and lip masses that expressed as the greatest population in this study, post-contrast HU numbers of both locations were not significantly different (125.60 ± 37.99 %, 71.80 – 195.60 % and 134.80 ± 51.51 %, 62.90 – 196.00% for gingival and lip masses, respectively; p = 0.7278). Similar results were detected at the clinical stages of oral tumors. The lower clinical stage of oral tumors (clinical stage 1 -2) revealed a slightly lower post-contrast HU number (126.06 ± 36.25 %; 62.90 – 196.00 %) than those of the higher clinical stage patients (clinical stage 3 – 4; 130.16 ± 49.52 %; 71.80 – 195.60 %) but a statistical difference was not detected (p = 0.8707).

Interestingly, tumor types having an effect on the CT value by means of SCC showed significantly higher post-contrast HU numbers (161.88 ± 23.47 %, 143.60 – 196.00%) than those for MM (122.78 ± 37.90%, 71.80 – 195.60%) and fibrosarcoma (99.37 ± 31.58%, 62.90 – 117.90%) (p < 0.05, Fig. 3).

Microvessel density: The mean MVD of the tumor tissue after immunohistochemical staining with vWF was 36.7 ± 11.7 vessels/mm^2 (range 19.7 – 54.6 vessels/mm^2). Similar results of the MVD number compared to the tumor locations and clinical stages were detected at the CT parameter and neither location nor clinical stage effected the MVD in tumor tissue. Considered by location, gingival masses revealed equal numbers of MVD (37.6 ± 12.4 vessels/mm^2, 21.2 – 54.6 vessels/mm^2) to those of lip masses (37.6 ± 13.0 vessels/mm^2, 19.7 – 51.3 vessels/mm^2; p = 0.9971). Likewise, the lower clinical stage of oral tumors (clinical stage 1 -2) revealed a slightly higher post-contrast HU number (38.2 ± 13.25 vessels/mm^2, 19.7 – 51.3 vessels/mm^2) than those of the higher clinical stage patients (clinical stage 3 – 4; 36.4 ± 11.6 vessels/mm^2, 21.1 – 54.6 vessels/mm^2) but a statistical difference was not detected (p = 0.7973).

Comparing different types of tumors, SCC showed significantly higher MVD values (47.5 ± 5.3 vessels/mm^2, 40.0 – 51.5 vessels/mm^2) than those found in MM (35.3 ± 11.6 vessels/mm^2, 21.2 – 54.6 vessels/mm^2) and fibrosarcoma (27.2 ± 6.5 vessels/mm^2, 19.7 – 31.9 vessels/mm^2) (p < 0.05, Fig. 4).

A comparison between the post-contrast enhanced HU attenuation number and the intratumor MVD showed significant correlation (R = 0.52, p < 0.01, Fig. 5).

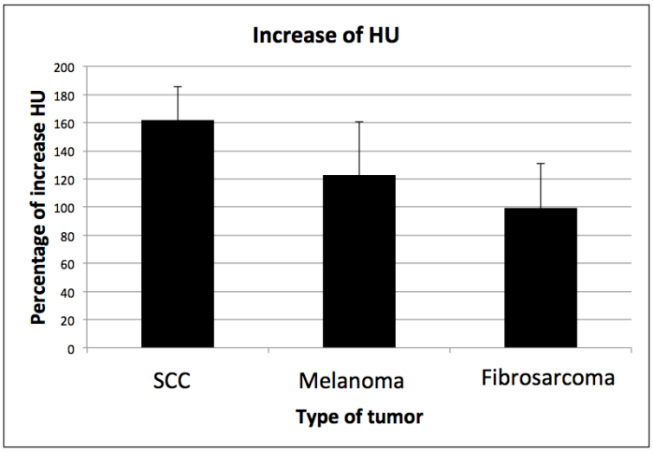

Figure 3 Post-contrast-enhanced computed tomographic (CT) Hounsfield Unit (HU) values for different types of canine oral tumor. Squamous cell carcinoma showed significantly HU than malignant melanoma or fibrosarcoma (P < 0.05).

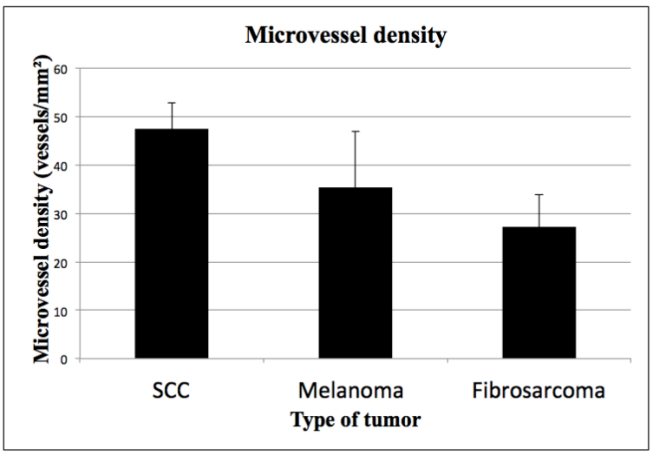

Figure 4 Intratumor microvessel density (MVD) values after immunohistochemical staining with vWF. The highest value of MVD was found in squamous cell carcinoma, followed by malignant melanoma and fibrosarcoma (P < 0.05).

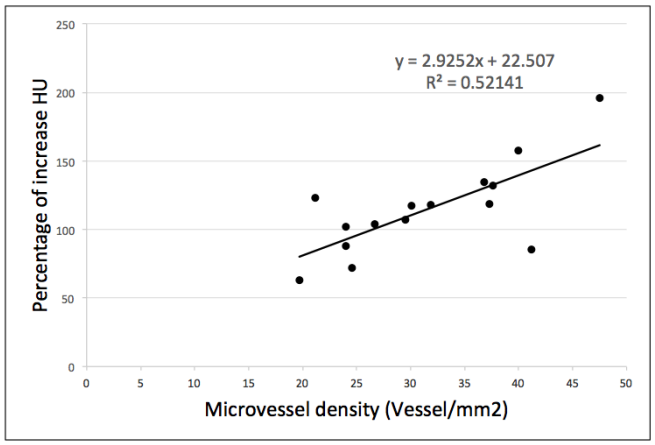

Figure 5 Statistically significant correlation between post-contrast-enhanced Hounsfield Units in the ROIs of the computed tomographic images and intra-tumor microvessel density ($P < 0.01$).

Discussion

CT image is an increasingly popular imaging modality for veterinary clinical diagnoses, especially in the areas of neurology (Iwamoto et al., 1993; Axlund and Hudson, 2003), orthopedics (Gemmill et al., 2005; Holsworth et al., 2005), soft tissue surgery, and veterinary oncology (Kafka et al., 2004). In addition to the plain or non-contrast enhanced CT image, it has been reported that an increase in post-contrast-enhanced CT density, as measured by HU value, has been correlated with an increased intratumoral MVD (Ouyang et al., 2017), which itself is a useful indicator of tumor malignancy. Therefore, the measurement of post-contrast enhanced HU in CT images has been suggested as a technique for the clinical investigation of tumor malignancy. Among locations, due to their complex structure, tumors involving the head and neck area are among the most difficult to examine pre-operatively, either by physical examination or using conventional imaging modalities such as radiography or ultrasonography, further imaging diagnostic modality such as utilization of CT images that can provide all of the structural changes such as tumor location, invasion and malignancy parameter, for example; the tumor angiogenesis in companion animal can be applied as the guideline to diagnosis, treatment and prognosis in clinical practice. Thus, the purpose of this study was to explore and compare tumor angiogenesis of canine oral tumors, evaluated using dynamic post-contrast-enhanced HU values and microvessel density.

In this study, to maximize the value of measuring intratumoral post-contrast HU among different sizes of canine patients, we designed the post-contrast CT protocol by drawing the ROI at the same anatomical level among different sizes of canine patients, instead of using duration setting methods as seen in other protocol such as the dynamic CT protocol commonly used for the liver (Fukushima et al., 2012). In our protocol, the mid-cervical jugular vein was selected to draw the ROI instead of the common carotid artery used in other CT protocols for the head and neck area because we wanted to make sure that the contrast medium circulated to the vascular bed of the oral tumor prior obtaining the post-contrast CT data. The goal was to improve the comparability of post-contrast enhancement measurements of oral tumors among canine patient of different sizes. In addition, with the goal of reducing the artifact in carotid CT angiography caused by contrast medium administration, we chose to administer the contrast medium into the right cephalic vein rather than the usual left forelimb injection site (Demirpolat et al., 2011). Also, compared to the previous dynamic contrast-enhanced CT image for predicting the tumor oxygenation in canine nasal tumor for which data were obtained from a single location scanning at various time periods (Camp et al., 2000) so that the results were sometimes hard to represent the whole neoplastic condition, our study was designed by whole area-CT scanning followed by picking up 5 randomized areas to represent the neovascularization through HU attenuation number. Therefore, the present study should be much more representative of the actual tumor angiogenesis in each tumor type.

Among 20 canine oral tumor patients in this study, our results were consistent with previous clinical demographic data in that most of the canine oral patients (Dorn and Priester, 1976; Vos and van der Gaag, 1987; Niemiec, 2008; Dobson, 2013).

Although our study revealed that tumor location and clinical staging did not count as a malignant factor effecting either of neovascularization or CT value in tumor tissue, those factors are currently debatable. It has been reported that the clinical stages of oral squamous cell carcinoma in human patients have been influenced to the MVD expression, especially in the early clinical stage (Wirsling et al, 2016). However, Rubin et al. (1999) reported that MVD expression was not significantly related to stage in other tumor type. By location, Dhanuthai et al (2013) additionally revealed that tumor site was not associated with MVD expression in salivary gland tumors but the tumor type did. Since there has been less information about the clinic-pathological parameters such as age gender, tumor stage and location that could effect the intraoral tumoral MVD expression and other tumor progressed parameters in companion animals such as dogs and cats, further study with a large group would unveil useful information.

After computed tomographic examination, tumors among MM, SCC and fibrosarcoma revealed slightly different characteristics. Most of the MM and fibrosarcoma canine patients showed a heterogeneous texture, whereas all of the SCC showed a homogeneous

pattern and almost all samples showed alike results as the histopathology samples. The result of SCC in canine patient was different from an earlier study of CT in feline SCC (Gendler et al., 2010). Although this study did not compare the MVD expression between normal and tumor tissues due to ethical issues, the HU in the tumor area was significantly higher than those of opposite intraoral normal tissue. In this study, either of MVD or HU was measured only in soft tissues, to avoid distortion of HU by including mineralization, which was scantly found in all patients and also to avoid at the necrotic tissue in all tumors. However, HU measurement in some areas might be done in the intratumoral granulation tissue due to poor detection of granulation tissue on the CT image than that of the MVD on histopathology. Although no previous study has examined neovascularization examined using dynamic CT or MVD, it has been reported that tumor angiogenesis evaluated by vascular endothelium growth factor (VEGF) expression was highest in SCC and lowest in fibrosarcoma (Sobszynkska-Rak et al., 2014), which is consistent with our observations. SCC is not the most common type of oral tumor in canine patients, but it is among the most malignant. Tumor angiogenesis in canine SCC might be up-regulated by several molecular pathways. One of the most notorious molecules important for tumor angiogenesis is cyclooxygenase II. It has been reported that SCC involves high COX II expression (Mohammed et al., 2004). Therefore, further investigation of tumor angiogenesis, including possible anti-angiogenesis treatment in SCC, might be helpful in clinical practice. Due to the small sample size of canine patients which is one of the limitation, and the fact that other malignancy parameters such as the proliferative index (PI) and survival period of each canine patient were not quantified in this study, further investigation on a larger scale would clearly be useful.

In conclusion, contrast enhanced CT HU on oral tumor imaging in dogs correlates to tumor microvascular density and may be useful as a less invasive indicator of neovascularization and malignancy.

Conflict of interest: There is no conflict of interest on this study.

Acknowledgements

This research was supported by the Scholarship from the Graduate School, Chulalongkorn University to Commemorate the 72nd Anniversary of His Majesty King Bhumibol Aduladej and a Graduate Thesis Grant, Graduate School, Chulalongkorn University.

References

Axlund TW and Hudson JA 2003. Computed tomography of the normal lumbosacral inter vertebral disc in 22 dogs. Vet Radiol Ultrasound. 44(6): 630 – 634.

Camp SV, Fisher P and Thrall DE 2000. Dynamic CT measurement of contrast medium washin kinetics in canine nasal tumors. Vet Radiol Ultrasound. 41(5): 403 – 408.

Codner EC, Lurus AG, Miller JB, Gavin PR, Gallina A, Barbee DD 1993. Comparison of computed tomography with radiography as a noninvasive diagnostic technique for chronic nasal disease in dogs. J Am Vet Med Assoc. 202(7): 1106 – 1110.

Demirpolat G, Yuksel M, Kavukçu G and Tuncel D 2011. Carotid CT angiography: Comparison of image quality for left versus right arm infections. Diagn Interv Radiol. 17(3):195 – 198.

Dhanuthai K, Sappayatosok K, Yodsanga S, Rojanawatsirivej S, Pausch NC and Pitak-Arnnop P 2013. An analysis of microvessel density in salivary gland tumours: a single centre study. The Surgeon II. 147 – 152.

Dobson J 2013. Breed-predispositions to cancer in pedigree dogs. ISRN Vet Sci. 2013: 941275.

Dorn CR and Priester WA 1976. Epidemiologic analysis of oral and pharyngeal cancer in dogs, cats, horses, and cattle. J Am Vet Med Assoc. 169(11): 1202 – 1206.

Drees R, Forrest LJ and Chappell R 2009. Comparison of computed tomography and magnetic resonance imaging for the evaluation of canine intranasal neoplasia. J Small Anim Pract. 50(7): 334 – 340.

Fukushima K, Kanemoto H, Ohno K, Takahashi M, Nakashima K, Fujino Y, Uchida K, Fujiwara R, Nishimura R and Tsujimoto H 2012. CT characteristics of primary hepatic mass lesions in dogs. Vet Radiol Ultrasound. 53(3): 252 – 257.

Gemmill TJ, Mellor DJ, Clements DN, Clarke SP, Farrell M, Bennett D and Carmichael S 2005. Evaluation of elbow incongruency using reconstructed CT in dogs suffering fragmented coronoid process. J Small Anim Pract. 46(7): 327 – 333.

Gendler A, Lewis JR, Reetz JA and Schwarz T 2010. Computed tomographic features of oral squamous cell carcinoma in cats: 18 cases (2002 – 2008). J Am Vet Med Assoc. 236(3): 319 – 235.

Ghirelli CO, Villamizar LA and Pinto ACBCF 2013. Comparison of standard radiography and computed tomography in 21 dogs with maxillary masses. J Vet Dent. 30(2): 72 – 76.

Holsworth IG, Wisner ER, Scherrer WE, Filipowitz D, Kass PH, Pooya H, Larson RF, Schulz KS 2005. Accuracy of computed tomographic evaluation of canine radio-ulnar incongruence in vitro. Vet Surg. 34(2): 108 – 113.

Iwamoto KS, Norman, A, Freshwater DB, Ingram M and Skillen RG 1993. Diagnosis and treatment of spontaneous canine brain tumors with a CT scanner. Radiother Oncol. 26(1): 76 – 78.

Kafka UC, Carstens A, Steenkamp G and Symington H 2004. Diagnostic value of magnetic resonance imaging and computed tomography for oral masses in dog. J S Afr Vet Assoc. 75(4): 163 – 168.

Miles KA, Lee TY, Goh V, Klotz E, Cuenod C, Bisdas S, Groves AM, Hayball MP, Alonzi R and Brunner T 2012. Current status and guidelines for the assessment of tumour vascular support with dynamic contrast-enhanced computed tomography. Eur Radiol. 22(7): 1430 – 1441.

Mohammed SI, Khan KN, Sellers RS, Hayek MG, DeNicola DB, Wu L, Bonney PL and Knapp DW 2004. Expression of cyclooxygenases-1 and 2 in naturally-occurring canine cancer. Prostaglandins Leukot Essent Fatty Acids. 70(5): 479 – 483.

Niemiec BA 2008. Oral pathology. Top Companion Anim Med. 23(2): 59 – 71.

Ohlerth S and Scharf G 2007. Computed tomography in small animals-basic principles and state of the art applications. Vet J. 173(2): 254 – 271.

Ouyang AM, Wei ZL, Su XY, Li K, Zhao D, Yu DX and Ma XX 2017. Relative computed tomography (CT) enhancement value for the assessment of microvascular architecture in renal cell carcinoma. Med Sci Monit. 31: 3706 – 3714.

Restucci B, Maiolino P, Paciello O, Martano M, De Vico G and Papparella S 2003. Evaluation of angiogenesis in canine seminoma by quantitative immunohistochemistry. J Comp Pathol. 128(4): 252 – 259.

Rubin MA, Buyyounouski M, Bagiella E, Sharir S, Neugut A, Benson M, Taille A, Katz AE, Olsson CA and Ennis RD 1999. Microvessel density in prostate cancer: lack of correlation with tumor grade, pathologic state, and cilinical outcome. Urology. 53(3): 542 – 547.

Sobczynkska-Rak A, Polkowska I and Silmanowicz P 2014. Elevated vascular endothelial growth factor (VEGF) levels in the blood serum of dogs with malignant neoplasm of the oral cavity. Acta Vet Hung. 62(3): 362 – 371.

Vos JH and van der Gaag I 1987. Canine and feline oral-pharyngeal tumours. J Vet Med Series A. 34(6): 420 – 427.

Weidner N 1995. Current pathologic methods for measuring intratumoral microvessel density within breast carcinoma and other solid tumors. Breast Cancer Res Treat. 36(2): 169 – 180.

Wolfesberger B, Tonar Z, Witter K, Guija de Arespacohaga A, Skalicky M, Walter I, Thalhammer JG and Egger GF 2008. Microvessel density in normal lymph nodes and lymphomas of dogs and their correlation with vascular endothelial growth factor expression. Res Vet Sci. 85(1): 56 – 61.

Wirsing AM, Rikardsen OG, Steigen SE, Uhlin-Hansen L and Hadler-Olsen E 2016. Present of tumour high-endothelial venules is an independent positive prognostic factor and stratifies patients with advanced-stage oral squamous cell carcinoma. Tumour Biol. 37(2): 2449 – 2259.

บทคัดย่อ

การศึกษาการเปรียบต่างของระดับสารเพิ่มความชัดภาพบนภาพรังสีส่วนตัดอาศัยคอมพิวเตอร์และการกำเนิดหลอดเลือดใหม่ในเนื้องอกช่องปากของสุนัข

อุราภา กลั่นเสนาะ[1] วิจิตร บรรลุนารา[2] แนน ช้อยสุนิรชร[1*]

การศึกษาครั้งนี้เป็นการศึกษาการเพิ่มขึ้นของระดับสารเพิ่มความชัดภาพบนภาพรังสีส่วนตัดอาศัยคอมพิวเตอร์เพื่อช่วยในการวินิจฉัยโรคเนื้องอกภายในช่องปากของสุนัข ผ่านการศึกษาความสัมพันธ์ ระหว่างความหนาแน่นของการเพิ่มขึ้นของสารเปรียบต่างบนภาพรังสีร่วมกับการเพิ่มขึ้นจำนวนหลอดเลือดฝอยภายในเนื้องอกช่องปาก โดยทำการศึกษาในสุนัขจำนวน 20 ตัวที่มีเนื้องอกในช่องปาก สุนัขดังกล่าวมีอายุระหว่าง 8 - 17 ปี น้ำหนักตัวระหว่าง 3.6 - 40.0 กิโลกรัม โดยสุนัขจำนวน 13 ตัวป่วยด้วยมะเร็งเม็ดสี สุนัขจำนวน 4 ตัวป่วยด้วยมะเร็งสแควร์มัสเซลล์ และสุนัขจำนวน 3 ตัวป่วยด้วยมะเร็งไฟโบรซาโครมา ผลการศึกษาพบระยะเวลาระหว่างการฉีดสารเพิ่มความชัดภาพบริเวณหลอดเลือดดำขาหน้าจนกระทั่งสารเพิ่มความชัดภาพเดินทางถึงบริเวณหลอดเลือดดำใหญ่บริเวณกลางคอที่ตำแหน่งกระดูกสันหลังส่วนคอชิ้นที่ 4 มีความสัมพันธ์กับน้ำหนักตัวของสัตว์ป่วย ($p < 0.01$) ค่าเฉลี่ยการเพิ่มขึ้นของสารเพิ่มการชัดภาพในในเนื้อเยื่อช่องปากมีค่าเท่ากับ 127.09 ± 38.58 % โดยพบค่าสูงที่สุดในมะเร็งสแควร์มัสเซลล์ (166.88 ± 23.47%, $p < 0.05$) ตามมาด้วยมะเร็งเม็ดสี (122.78 ± 37.90%) และมะเร็งไฟโบรซาโครมา (99.37 ± 31.58%) ตามลำดับ ค่าเฉลี่ยการเพิ่มขึ้นของจำนวนความหนาแน่นหลอดเลือดขนาดเล็กในเนื้องอกผ่านการตรวจด้วยวิธีทางอิมมูโนฮีสโตเคมีด้วยโปรตีนวอนวิลลิแบรนด์มีค่าเท่ากับ 36.7 ± 11.7 หลอดเลือดต่อตารางมิลลิเมตร โดยค่าดังกล่าวมีค่าสูงสุดในมะเร็งสแควร์มัสเซลล์ (47.5 ± 5.3 หลอดเลือดต่อตารางมิลลิเมตร, $p < 0.05$) ตามมาด้วยมะเร็งเม็ดสี (35.3 ± 11.6 หลอดเลือดต่อตารางมิลลิเมตร) และมะเร็งไฟโบรซาโครมา (27.2 ± 6.5 หลอดเลือดต่อตารางมิลลิเมตร) ตามลำดับ พบความสัมพันธ์กันระหว่างความหนาแน่นของหลอดเลือดขนาดเล็กและการเพิ่มขึ้นของระดับสารเพิ่มความชัดภาพบนภาพรังสีส่วนตัดอาศัยคอมพิวเตอร์อย่างมีนัยสำคัญทางสถิติ ($p < 0.01$)

คำสำคัญ: การกำเนิดหลอดเลือดใหม่ ภาพถ่ายรังสีส่วนตัดอาศัยคอมพิวเตอร์ สุนัข ช่องปาก เนื้องอก

[1]ภาควิชาศัลยศาสตร์ คณะสัตวแพทยศาสตร์ จุฬาลงกรณ์มหาวิทยาลัย ปทุมวัน กรุงเทพ ฯ 10330

[2]ภาควิชาพยาธิวิทยา คณะสัตวแพทยศาสตร์ จุฬาลงกรณ์มหาวิทยาลัย ปทุมวัน กรุงเทพ ฯ 10330

****ผู้รับผิดชอบบทความ** E-mail: nan.c@chula.ac.th*